Available online at www.sciencedirect.com
ScienceDirect
Ocean Modelling 15 (2006) 71–89
Ocean Modelling
www.elsevier.com/locate/ocemod

An unstructured grid morphodynamic model with a discontinuous Galerkin method for bed evolution

Ethan J. Kubatko [a,*], Joannes J. Westerink [a], Clint Dawson [b]

[a] *Department of Civil Engineering and Geological Sciences, University of Notre Dame, Notre Dame, IN 46556, United States*
[b] *Institute for Computational Engineering and Sciences, The University of Texas at Austin, Austin, TX 7871, United States*

Received 2 February 2005; received in revised form 24 April 2005; accepted 4 May 2005
Available online 5 July 2005

Abstract

A new unstructured grid two-dimensional, depth-integrated (2DDI), morphodynamic model is presented for the prediction of morphological evolutions in shallow water. This modelling system consists of two coupled model components: (i) a well-verified and validated continuous Galerkin (CG) finite element hydrodynamic model; and (ii) a new sediment transport/bed evolution model that uses a discontinuous Galerkin (DG) method for the solution of the sediment continuity equation. The DG method is a robust finite element method that is particularly well suited for this type of advection dominated transport equation. It incorporates upwinded numerical fluxes and slope limiters to provide sharp resolution of steep bathymetric gradients that may form in the solution, and it possesses a local conservation property that conserves sediment mass on an elemental level. In this paper, we focus specifically on the implementation and verification of the DG model. Details are given on the implementation of the method, and numerical results are presented for three idealized test cases which demonstrate the accuracy and robustness of the method and its applicability in predicting medium-term morphological changes in channels and coastal inlets.

* Corresponding author.
E-mail addresses: ekubatko@nd.edu (E.J. Kubatko), jjw@photius.ce.nd.edu (J.J. Westerink), clint@ices.utexas.edu (C. Dawson).

1463-5003/$ - see front matter © 2005 Elsevier Ltd. All rights reserved.
doi:10.1016/j.ocemod.2005.05.005

1. Introduction

The transport of sediment as bed load is an important process that occurs in rivers, estuaries, and coastal regions. In many situations, this process and the resulting morphological changes of the bed can have a detrimental impact on the coastal infrastructure and environment. For example, dredged navigational channels and coastal inlets can be rendered almost entirely useless by the accumulation of transported sediment. Returning these structures to operational status, through dredging operations or the construction of jetties, represents a significant cost to the agencies that maintain them. As another example, the structural integrity of bridges and piers may be compromised due to excessive scour of the bed around abutments. In addition to these infrastructure problems, there is host of environmental issues of concern, such as the transport of pollutants with or as sediment, that can cause serious ecological damage. Accurate numerical models that can predict sediment transport and the resulting bed morphology can help manage these costly problems.

Clearly, the processes of sediment transport and morphological evolution of the bed are determined by the properties of the fluid flow, which in turn are affected by the changes in the morphology of the bed that they induce. Thus, the motion of the fluid and the motion of the bed form an interdependent two-phase phenomenon that must be analyzed using a model *system* made up of two distinct but interdependent model *components*: (i) a hydrodynamic component defining the evolution of the flow; and (ii) a sediment transport/morphological component defining the evolution of the bed. Such a modelling system is often referred to as a morphodynamic model. A description and comparison of some existing morphodynamic model systems is given by Nicholson et al. (1997). Typically, these model systems use structured computational grid methods. To a lesser extent, unstructured grid methods have also been implemented and can, in fact, be highly advantageous based on their ability to provide local grid refinement near important bathymetric features and structures. The ability to provide local grid refinement where it is needed leads to improved accuracy for a given computational cost as compared to models that use structured grid methods. However, both structured and unstructured grid method solutions to the governing morphological equation can experience numerical robustness and accuracy problems manifested in the form of spurious spatial oscillations, especially in the presence of steep bathymetric gradients (see for example Johnson and Zyserman, 2002).

In this paper, we describe the development of a new unstructured grid morphodynamic model system that uses a new class of highly accurate finite element methods for the solution of the governing morphological equation. The hydrodynamic model component of our system is provided by the well-verified and validated unstructured grid model ADCIRC, developed by the second author and a number of collaborators (Luettich and Westerink, 2004). ADCIRC is both a two-dimensional, depth-integrated (2DDI) and three-dimensional (3D) free surface flow model. In this paper, we focus specifically on the 2DDI ADCIRC model, which solves the shallow water equations using the standard or continuous Galerkin (CG) finite element method in space. To overcome well-known problems in solving the shallow water equations using equal-order interpolating spaces with the CG finite element method, the continuity equation is replaced by the so-called generalized wave continuity equation (GWCE) (Lynch and Gray, 1979; Kinnmark, 1986). The solution strategy used in ADCIRC has proven to be robust and computationally

efficient, and it has been validated in a large number of cases (see for example Blain et al., 1994; Westerink et al., 1994, in review; Mukai et al., 2002).

Working with a well-established hydrodynamic model then, the main focus of this paper is the development and verification of a bed load sediment transport/morphological model component to work in conjunction with ADCIRC. Mathematically, the morphological evolution of the bed is defined by the so-called sediment continuity or Exner equation. This equation simply states that the time rate of change of the bed elevation is equal to the divergence of the sediment flux, which can be expressed in terms of the local flow properties through the use of an empirical sediment transport formula. As is well known, solving advection dominated transport equations of this type using the CG finite element method will frequently lead to spurious spatial oscillations in the solution. To overcome these shortcomings, a number of so-called advection schemes can be employed (see Iskandarani et al., 2005 for a review and comparison of some of the more popular schemes). One such scheme that has received considerable recent attention and that has been applied successfully to a wide variety of problems is the discontinuous Galerkin (DG) finite element method.

Originally developed by Reed and Hill (1973), but more recently expounded on in a series of papers by Cockburn et al. (see the review article by Cockburn and Shu, 2001 and the references therein), the DG method uses trial and test function spaces that are continuous over a given element but which allow discontinuities between elements. This results in a block diagonal or, with an appropriate choice of basis, diagonal mass matrix that can be trivially inverted. Communication between elements is accomplished via a so-called numerical flux, which for the case of a scalar equation can be defined using upwinding techniques. The method is also ''locally conservative'', meaning that the conservation of the transported quantity is satisfied on a local or elemental level. This has been shown to be a desirable property when coupling flow and transport algorithms (see for example Dawson et al., 2004).

In this paper, we present the implementation and verification of a DG sediment transport/morphological model that is coupled to the ADCIRC hydrodynamic model. We note that this sediment transport model is just one component of a suite of DG model components that are currently being developed for flow and transport, which will form a completely DG based morphodynamic modelling system with both h (grid size) and p (polynomial order) refinement options. In this paper, we restrict our attention to the second-order ($p = 1$) case for the sediment transport model, but we note that p-refinement is easily implemented within the framework of the DG method (see Kubatko et al., in preparation for an example of this for the shallow water equations).

This paper is organized as follows. In Section 2, we describe the mathematical model defining the sediment transport and morphological evolution of the bed which consists of the sediment continuity equation and an empirical sediment transport formula. We then present a simplified mathematical model, which we refer to as the Exner model, that uncouples the sediment transport/morphological model from the hydrodynamic model. This simplified model can be used as a verification tool for the numerical method. In Section 3, we give a detailed description of our implementation of the DG method for the sediment continuity equation, giving specific details on the numerical flux, basis, quadrature rules, time discretization, slope limiter, and continuous projection that are employed. In Section 4, we present numerical results from three test cases with

the aim of: (i) verifying that the method achieves second-order convergence in space; and (ii) demonstrating how the model can be used for predicting so-called medium-term (see for example De Vriend et al., 1993) morphological changes in channels and coastal inlets. Finally, in Section 5, we summarize this paper, and we briefly discuss the current and future work in the development of this model system.

2. Mathematical model

The evolution of the bed or bottom surface elevation due to the transport of sediment as bed load is governed by the so-called sediment continuity or Exner equation (see for example Henderson, 1966):

$$\frac{\partial z}{\partial t} + \nabla \cdot \mathbf{q}_b = 0 \tag{1}$$

where z is the elevation of the bed relative to a datum located below the bed (z is positive upwards) and $\mathbf{q}_b$ is the bed load sediment transport function vector.

In order to close Eq. (1), a functional form of $\mathbf{q}_b$ must be specified. It is assumed that the sediment transport is always in the direction of the flow velocity, $\mathbf{U} = (u, v)$ where u and v are the velocity components of the flow in the x and y directions, respectively. Thus the vector $\mathbf{q}_b$ is computed as

$$\mathbf{q}_b = \widehat{\mathbf{U}}|\mathbf{q}_b| \tag{2}$$

where $|\mathbf{q}_b|$ is the magnitude of the sediment transport in the direction of the flow and $\widehat{\mathbf{U}}$ is the normalized flow velocity vector (i.e. $\widehat{\mathbf{U}} = \mathbf{U}/|\mathbf{U}|$). There are a number of empirical bed load sediment transport functions available (e.g. Bagnold, Einstein, Meyer-Peter and Mueller, see for example Sleath, 1984 for a thorough list), most of which can be transcribed in the following form:

$$|\mathbf{q}_b| = A(\mathbf{U}, H, \ldots)|\mathbf{U}|^n \tag{3}$$

where A is a given function and n is a given positive constant both of which are specific to the particular sediment transport formula. Note that A is typically a function of the flow velocity, $\mathbf{U}$, the total height of the water column, $H = \zeta - z$ (where ζ is the water surface elevation relative to the same datum as the bed), and a number of constants that are based on sediment properties such as sediment type and grain size and data fitting procedures. The constant n is typically in the range of $1 \leqslant n \leqslant 3$.

In our model, we will make use of a new bed load formula developed by Camenen and Larson (2005), though the numerical model to be described will be general enough to allow the use of any sediment transport formula provided it is a function of H and a monotonically increasing function of $\mathbf{U}$. Camenen and Larson develop new bed load sediment transport formulas for transport due to currents, waves, and combined waves and currents. Their formulas were shown to provide the best agreement with the data sets that were compiled compared to a number of previously proposed formulas (Camenen and Larson, 2005).

In this paper, we only consider the Camenen and Larson bed load sediment transport formula due to currents which is given by (in dimensional form—SI units):

$$|q_b| = C\tau_c^{1.5} \exp\left(-4.5\frac{\tau_{cr}}{\tau_c}\right) \tag{4}$$

where τ_c is the shear stress at the bottom due to the current, τ_{cr} is the critical shear stress, and C is a constant given by

$$C = \frac{12}{g\sqrt{\rho}(\rho_s - \rho)} \tag{5}$$

where g is the acceleration due to gravity and ρ and ρ_s are the water and sediment density, respectively. The shear stress is computed by the formula:

$$\tau_c = \frac{1}{2}\rho f |\mathbf{U}|^2 \tag{6}$$

where f is a dimensionless friction factor calculated assuming a logarithmic velocity profile (see for example Sleath, 1984):

$$f(H) = \frac{8}{25}\left[1 + \ln\left(\frac{d_{50}}{15H}\right)\right]^{-2} \tag{7}$$

where d_{50} is the median grain size. The critical shear stress is computed from the critical Shields parameter which is either estimated as a constant or calculated using the formula proposed by Soulsby and Whitehouse (1997).

Using Eqs. (5)–(7) the sediment transport formula can be written in the form of Eq. (3) with $n = 3$ and A given by the function:

$$A = C\left(\frac{1}{2}\rho f\right)^{1.5} \exp\left(-4.5\frac{\tau_{cr}}{\tau_c}\right) \tag{8}$$

Note that A is a monotonically increasing function of τ_c and therefore $\mathbf{U}$.

2.1. A simplified model

For purposes of verifying our numerical scheme, we use a simplified mathematical model that essentially uncouples the sediment continuity equation from the hydrodynamics. This allows us to verify the underlying numerics of the model in a simplified setting by comparing it to analytical solutions. Assume that the flow is unidirectional (say in the x directional only) and quasi-steady with a rigid lid. With these assumptions, the flow velocity is given by

$$u = \frac{q_f}{H} = \frac{q_f}{\bar{\zeta} - z} \tag{9}$$

where q_f is a constant flow discharge and $\bar{\zeta}$ is the elevation of the rigid lid measured from the bed datum (see Fig. 1). Furthermore, assume that the sediment transport is given by Eq. (3) with $A =$ constant and $n = 1$. With these assumptions the sediment continuity equation can be written as

$$\frac{\partial z}{\partial t} + \frac{\partial}{\partial x}\left(A\frac{q_f}{\bar{\zeta} - z}\right) = 0 \tag{10}$$

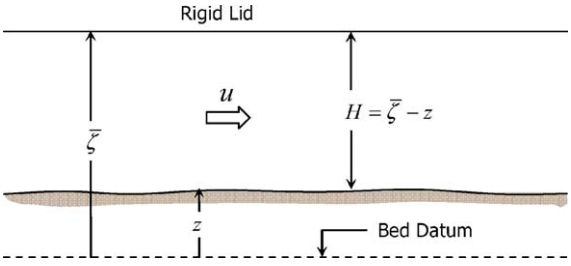

Fig. 1. Definition sketch for Exner's model.

This model was originally proposed by Exner (1925). Assuming a smooth initial condition, $z(x, 0) = z_0$, the classical solution is given implicitly by

$$z(x,t) = z_0(x - c_z t), \quad c_z = Aq_f/(\bar{\zeta} - z)^2 \tag{11}$$

where c_z is the propagation speed of the bed. As is well known, non-linear hyperbolic equations such as Eq. (10), depending on the initial conditions, will develop steep gradients (and eventually discontinuities or shocks) which provide a rigorous test for a numerical method. A similar model was examined by Johnson and Zyserman (2002) in the context of testing a finite difference scheme.

3. Numerical model

In this section, we give a detailed description of our DG sediment transport/morphological model. To begin we define some notation. Given a spatial domain, Ω, which has been discretized into a set of non-overlapping elements, let Ω_e define the domain of a typical element e and denote the boundary of the element by Γ_e. Our numerical approximation of z will make use of piecewise smooth functions which are continuous over Ω_e but which allow discontinuities between elements along a given edge. We denote this space of functions by V_h. Given a smooth function v defined over e, we denote the values of v along an edge by $v^{(\text{in})}$ when approaching the edge from the interior of the element and $v^{(\text{ex})}$ when approaching the edge from the exterior of the element. The outward unit normal vector for the boundary of the element will be denoted by $\mathbf{n}$, and the fixed unit normal vector for a given edge i will be denoted by $\mathbf{n}_i$ (see Fig. 2).

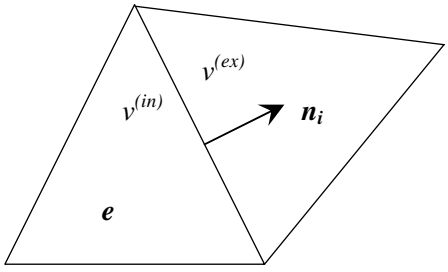

Fig. 2. A typical element e and its neighboring element along edge i with normal $\mathbf{n}_i$; $v^{(\text{in})}$ and $v^{(\text{ex})}$ denote the value of a function v along edge i when approaching the edge from the interior and exterior of the element, respectively.

In our numerical scheme, we will also make use of continuous, piecewise linear approximations of $\mathbf{U}$ and ζ obtained from the ADCIRC model to compute the local sediment transport rates. Briefly, these approximations are obtained by solving the shallow water equations using the CG finite element method in space and implicit/explicit time stepping (see Luettich and Westerink, 2004 for details). As previously mentioned, to achieve non-oscillatory results the primitive continuity equation is replaced with the GWCE.

We apply the DG method to the sediment continuity equation by multiplying Eq. (1) by a test function $v \in V_h$ and integrating over Ω_e to obtain

$$\int_{\Omega_e} \frac{\partial z}{\partial t} v \, \mathrm{d}\Omega_e + \int_{\Omega_e} \nabla \cdot \mathbf{q}_\mathrm{b} v \, \mathrm{d}\Omega_e = 0 \tag{12}$$

Integrating the second term of this equation by parts gives

$$\int_{\Omega_e} \frac{\partial z}{\partial t} v \, \mathrm{d}\Omega_e - \int_{\Omega_e} \nabla v \cdot \mathbf{q}_\mathrm{b} \, \mathrm{d}\Omega_e + \int_{\Gamma_e} v \mathbf{q}_\mathrm{b} \cdot \mathbf{n} \, \mathrm{d}\Gamma_e = 0 \tag{13}$$

Next we replace the solution z with an approximate solution z_h which, using Galerkin's method, is constructed from a set of basis functions which belong to the same space, V_h, as the test functions. Due to the fact that there may be discontinuities along element edges, the boundary integral of Eq. (13) is undefined and for this we define a numerical flux, $\hat{q}_\mathrm{b}$. In our formulation, we use a simple upwind flux based on the assumption that the sediment transport is in the direction of the current:

$$\hat{q}_\mathrm{b} = \begin{cases} \mathbf{q}_\mathrm{b}^{(\mathrm{in})} \cdot \mathbf{n}, & \mathbf{U} \cdot \mathbf{n} \geqslant 0 \\ \mathbf{q}_\mathrm{b}^{(\mathrm{ex})} \cdot \mathbf{n}, & \mathbf{U} \cdot \mathbf{n} < 0 \end{cases} \tag{14}$$

With the approximate solution and the numerical flux defined, the weak formulation of the problem now becomes

$$\int_{\Omega_e} \frac{\partial z_h}{\partial t} v \, \mathrm{d}\Omega_e - \int_{\Omega_e} \nabla v \cdot \mathbf{q}_\mathrm{b} \, \mathrm{d}\Omega_e + \int_{\Gamma_e} v \hat{q}_\mathrm{b} \, \mathrm{d}\Gamma_e = 0 \tag{15}$$

Note that the method is locally or elementally conservative in the following sense: setting $v = 1$ on Ω_e and zero elsewhere we have

$$\int_{\Omega_e} \frac{\partial z_h}{\partial t} \, \mathrm{d}\Omega_e + \int_{\Gamma_e} \hat{q}_\mathrm{b} \, \mathrm{d}\Gamma_e = 0 \tag{16}$$

That is, the time rate of change of z_h over Ω_e is balanced by the net flux of sediment into Ω_e.

We proceed by describing the details of the implementation of the scheme including the choice of basis functions, the quadrature rules employed to compute the integrals, the time discretization, the application of a slope limiter to eliminate local undershoots or overshoots in the solution in the presence of steep gradients, and the continuous projection procedure used to project the discontinuous approximation z_h into the space of continuous, piecewise linear functions which are fed back into ADCIRC as updated bathymetry.

3.1. Basis and degrees of freedom

As emphasized by Cockburn and Shu (1998), we note here that a judicious choice of basis functions can simplify the implementation of the scheme and improve the computational efficiency. Owing to the fact that discontinuities are permitted across element interfaces, the choice of the basis functions are not limited by the requirement of continuity as in the CG finite element method. Therefore, one can choose degrees of freedom that, for example, save cost in evaluating the integrals in Eq. (15) and/or simplify the implementation of the slope limiter. In our implementation, we use piecewise linear triangular elements described below.

Considering the "master element" as shown in Fig. 3 defined in the transformed coordinates ξ and η, the approximate solution z_h can be expressed as

$$z_h = \sum_{i=1}^{3} z_i(t)\phi_i(\xi,\eta) \tag{17}$$

where the degrees of freedom, z_i are the values of the approximate solution at the mid-point of each edge and the basis functions, ϕ_i define the linear element of Crouzeix and Raviart (1973) which for the master element shown in Fig. 3 can be written in the form:

$$\phi_1 = 1 - 2\xi, \quad \phi_2 = 1 - 2\eta, \quad \phi_3 = 2\xi + 2\eta - 1 \tag{18}$$

There are several things to note about this basis. The functions ϕ_i are equal to 1 at the mid-point of each edge i and 0 at the mid-points of the other two edges. The basis functions are orthogonal over an element, specifically

$$\int_{\Omega_m} \phi_i\phi_j \,\mathrm{d}\xi\,\mathrm{d}\eta = \begin{cases} 1/6, & i = j \\ 0, & i \neq j \end{cases} \tag{19}$$

where Ω_m denotes the domain of the master element. This property, of course, gives rise to an orthogonal mass matrix that can be trivially inverted. Lastly, in the continuous projection procedure to be described, we will make use of the value of the approximate solution at the vertices of

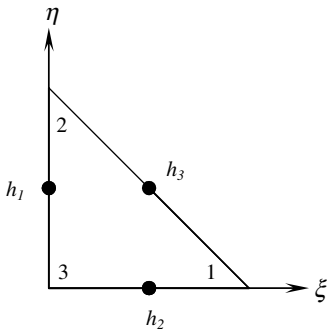

Fig. 3. Master element defined in local coordinates ξ and η showing the degrees of freedom h_i—the value of h at the midpoint of edge i opposite of corner node i.

the triangle. The value of z_h at vertex i, denoted by z_{vi}, which is the vertex opposite of edge i (see Fig. 3), is easily computed as

$$z_{vi} = -2z_i + \sum_{j=1}^{3} z_j \tag{20}$$

As a final note, we remark that the orthogonal, hierarchical, "modal" type basis proposed by Dubiner (1991), which simplifies p refinement and also adaptivity, can easily be implemented within the framework of the DG method.

3.2. Quadrature rules

Both of the integrals appearing in Eq. (15) are evaluated using suitable numerical quadrature rules. We note that by using numerical quadrature and the simple upwind numerical flux defined previously, we can easily implement a number of different sediment transport formulas into the scheme without making any changes to the base algorithm itself (provided that the formula meets the requirements as specified in Section 2). Cockburn and Shu (1998) note that for a DG spatial discretization of degree p, quadrature rules that are exact for polynomials of degree $2p$ and $2p+1$ must be used for the area and boundary integrals, respectively. Thus for the linear elements used here ($p = 1$) we use a three point quadrature rule for the triangle so the area integral of Eq. (15) is approximated by (noting that ∇v is constant over the element):

$$\nabla v \cdot \left(\int_{\Omega_e} \mathbf{q}_\mathrm{b} \, \mathrm{d}\Omega_e \right) \approx \nabla v \cdot \left(\sum_{i=1}^{3} w_i \mathbf{q}_\mathrm{b}(\mathbf{U}_i, \zeta_i, z_i) \right) \tag{21}$$

where the w_i's are the quadrature weights of the associated quadrature points, which are the mid-points of each edge. Using this rule, the sediment transport function, $\mathbf{q}_\mathrm{b}$ is easily evaluated at the quadrature points given the fact that we already have z_i, which are the degrees of freedom, and we need only to compute $\mathbf{U}$ and ζ at the mid-point of each edge. We note that these values are easily obtained by averaging the two vertices for the given edge (owing to the fact that $\mathbf{U}$ and ζ are approximated using linear functions over the element as well). The boundary integrals, which must integrate a third degree polynomial exactly, are evaluated using the two-point Legendre–Gauss quadrature rule.

3.3. Time discretization

The DG spatial discretization reduces the problem to a system of ordinary differential equations which we write in the concise form:

$$\frac{\mathrm{d}}{\mathrm{d}t}(\mathbf{z}_h) = L_h(\mathbf{z}_h, \mathbf{U}_h, \boldsymbol{\zeta}_h) \tag{22}$$

where $\mathbf{z}_h$ is the vector of unknowns over the whole domain.

We discretize this system of equations in time using a second-order Runge–Kutta scheme, which is equivalent to the so-called modified Euler method, written in the form:

$$\begin{aligned}\mathbf{z}_h^{(1)} &= \mathbf{z}_h^{(t)} + \Delta t_{\mathrm{m}} L_h\left(\mathbf{z}_h^{(t)}, \mathbf{U}_h^{(t)}, \boldsymbol{\zeta}_h^{(t)}\right)\\ \mathbf{z}_h^{(t+1)} &= \frac{1}{2}\left(\mathbf{z}_h^{(t)} + \mathbf{z}_h^{(1)} + \Delta t_{\mathrm{m}} L_h\left(\mathbf{z}_h^{(1)}, \mathbf{U}_h^{(t)}, \boldsymbol{\zeta}_h^{(t)}\right)\right)\end{aligned} \tag{23}$$

where Δt_{m} is the morphological time step which may be different than that of the hydrodynamic time step, Δt_{h}, and where it is to be noted that $\mathbf{U}$ and $\boldsymbol{\zeta}$ are held fixed at time t.

Given that explicit time stepping is used, the size of the morphological time step is limited by a Courant–Friedrichs–Levy (CFL) condition. A direct calculation of this condition proves difficult in practice due to the highly non-linear nature of the sediment transport function, and instead we simply take $\Delta t_{\mathrm{m}} = N \times \Delta t_{\mathrm{h}}$, where N is some positive integer usually in the range of 10–50, i.e. the bed is updated every 10–50 hydrodynamic time steps. In practice, this approach has proven to work well for a wide variety of problems and requires little additional computational effort. It has been estimated that using this approach the additional computational cost for running the morphodynamic model is on the order of 2–10% of the cost of running the hydrodynamic model alone.

3.4. Slope limiter

In order to prevent spurious oscillations at sharp fronts, a slope limiter is applied at each step of the Runge–Kutta method described above. We apply a simple slope limiter in which the degrees of freedom z_i for a given element e are compared to the average of the approximate solution over e, z^e_{avg} and the average of the neighboring element e' of the given edge, $z^{e'}_{\mathrm{avg}}$. If z_i does not fall in between the values z^e_{avg} and $z^{e'}_{\mathrm{avg}}$ for the given edge i then the degrees of freedom for element e are set equal to z^e_{avg}. In this way, the average of the element is maintained while setting its slope equal to zero, and sediment mass is still conserved over the element. It should be noted this slope limiter is very easy to implement, but it can cause some numerical smoothing of the solution. More sophisticated limiters that are less dissipative are currently being investigated.

We remark that for sufficiently smooth bathymetries, in practice it is often unnecessary to apply the limiter. However, as the bed evolves, steep gradients may develop in the bed, and it has been observed that without the use of a limiter oscillations develop in the neighborhood of the steep gradient. Typically, however, these oscillations seem to remain localized and do not degrade the solution globally. The role of the slope limiter then, at least for the problems examined, is that of a mechanism to eliminate local oscillations rather than for stabilizing the scheme.

3.5. Continuous projection procedure

As previously mentioned, ADCIRC makes use of approximations that are continuous in space across the entire domain. Thus, in addition to our discontinuous approximation $\mathbf{z}_h$, we must also compute a continuous approximation which must be fed back into ADCIRC after computing the updated bathymetry. We wish to accomplish the following with our procedure: given a node j which is a vertex for n different elements we wish to compute a single nodal value denoted by $\bar{z}_j$ based on the n (possibly) unique values at that node that are obtained from the DG method

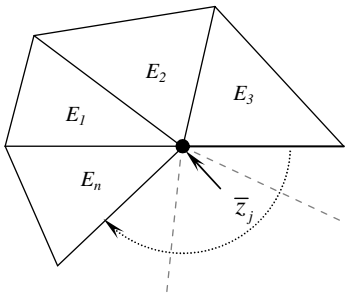

Fig. 4. Node j surrounded by n elements; the continuous approximation $\bar{z}_j$ for node j is determined from the (possibly) n unique values from the elements surrounding the node.

within the individual elements attached to that node (see Fig. 4). We have experimented with several different approaches for obtaining these single nodal values and based on numerical experiments have implemented an angle based weighted average given by

$$\bar{z}_j = \sum_{i=1}^{n} \left(\frac{\angle_i}{\angle_{\mathrm{SUM}}} z_{vi} \right) \tag{24}$$

where $\angle_i$ is the angle of the vertex of element i and $\angle_{\mathrm{SUM}}$ is the total sum of the vertex angles around node j. We have also experimented with weighted area averaging and centroidal type averaging, but we have found that the approach given by Eq. (24) gives the most consistent results under a wide variety of grid configurations. We note that under certain grid configurations it was observed that mild in-plane (x–y plane) oscillations appeared in the continuous representation of the bed. The weighted angle approach minimized the appearance of these oscillations, which were often much more visible using other averaging techniques. It should be noted this procedure does not affect the local conservation property of the sediment due to the fact that $\bar{z}$ is not actually used in the computations for updating the bed.

4. Numerical results

The DG method outlined above has been applied to a number of problems. In this section, we show the results for three idealized test cases.

4.1. Test Case 1: Morphological evolution of a symmetric mound

In this test case, we apply the DG method outlined above to the Exner model introduced in Section 2. The Exner model is examined in order to verify the numerical method independently of the hydrodynamic model. It also affords us the opportunity to compare our numerical results to exact solutions so that we may check the order of convergence of the method.

We solve a problem originally posed by Exner (1925). The problem examines the evolution of an initially symmetric mound subjected to steady, unidirectional flow with a rigid-lid assumption for the flow. The initial condition is given as

$$z(x,y,0) = z_0(x,y) = A_0 + A_1 \cos\left(\frac{2\pi x}{\lambda}\right) \tag{25}$$

where the parameters A_0, A_1 , and λ are as defined in Fig. 5 which shows a cross section of the mound along the x-axis. We take $A_0 = A_1 = 1$, $\lambda = 20$ in Eq. (25) and $\bar{\zeta} = 3$, $Aq_f = 1$ in Eq. (10). The flow is assumed to be in the x direction only, and we use periodic boundary conditions, i.e. $z(x = -\lambda/2, y) = z(x = +\lambda/2, y)$ and $z(x, y = -\lambda/2) = z(x, y = +\lambda/2)$. The exact solution is given by Eq. (11).

We solve this one-dimensional problem over a two-dimensional domain using four different grids with uniform nodal spacing of $h = 1$, 0.5, 0.25, and 0.125. We compute the maximum or L_∞ norm by comparing our DG solutions to the exact solution. In Fig. 6, we plot h versus the maximum error norm on a log–log scale where it can be observed that the theoretical convergence rate of $p + 1$ is obtained. Both the numerical and exact solutions of the evolution of the mound at a cross section taken along the x-axis are shown at two different times in Fig. 7. The solutions indicate that the mound develops into a dune-like shape with a gentle upstream slope followed by a steeper downstream slope that becomes progressively steeper in time. It should be noted

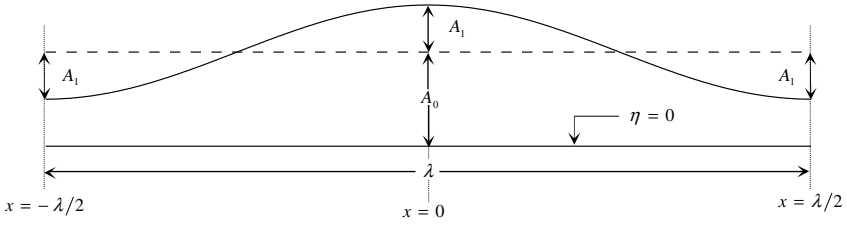

Fig. 5. Cross section of the initial condition for Exner's "dune problem" as defined by Eq. (25).

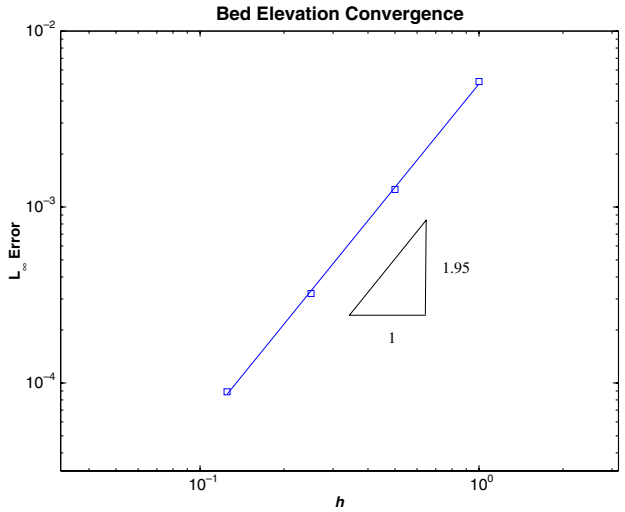

Fig. 6. Convergence plot of test case 1 demonstrating second-order convergence.

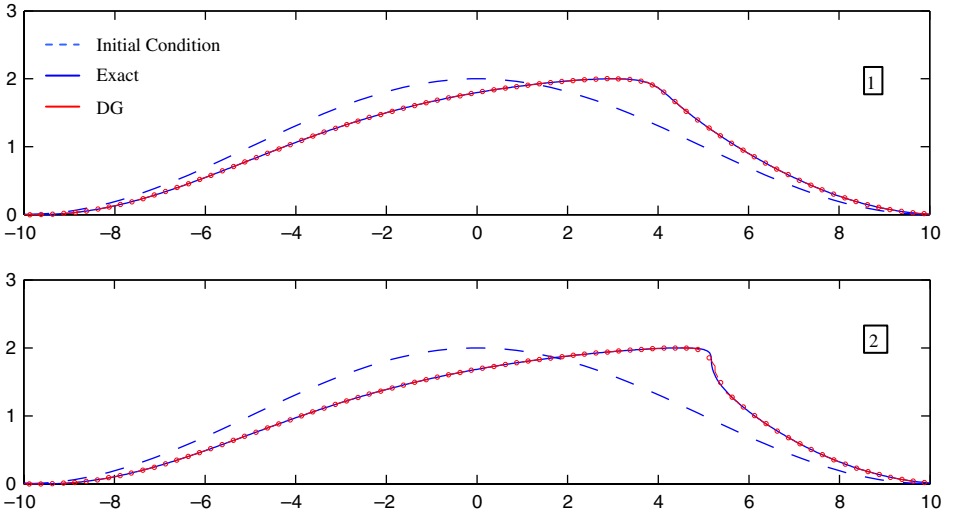

Fig. 7. Comparison of the exact and DG solution for test case 1.

how well the DG solution captures the steep downstream slope of the dune without the introduction of any spurious spatial oscillations or any significant numerical damping.

4.2. Test Case 2: Converging channel

In this problem, we return to the full morphodynamic modelling system and examine the morphological evolution of an initially flat bed in a converging channel. A plan view of the channel showing the computation grid is shown in Fig. 8. The channel tapers in from a maximum width of 500 m at the edges to 250 m in the center over a distance of 2 km. The boundary conditions for the hydrodynamics are specified in such a way that a maximum velocity of approximately 1 m/s occurs in the center of the channel. The evolution of the bed is examined over a 90-day period. The sediment density and median grain size of the bed are taken to be 2000 kg/m^3 and 0.2 mm, respectively. The time step used in the hydrodynamic model is 2 s and the bed is updated every 50 hydrodynamic time steps. Figs. 9a–c show plots of the bed elevation surface and velocity contours at 30, 60, and 90 days. The bed changes have been scaled in the vertical for easy visualization.

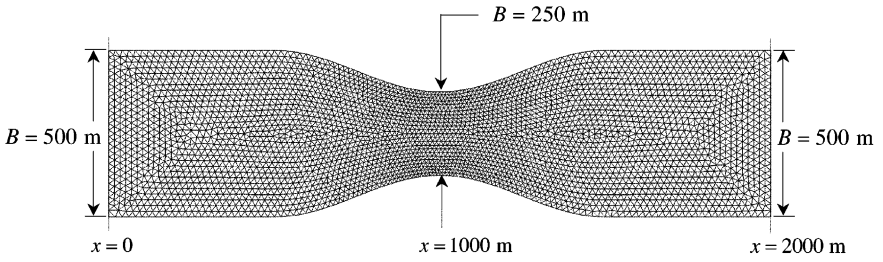

Fig. 8. Computational grid of test case 2.

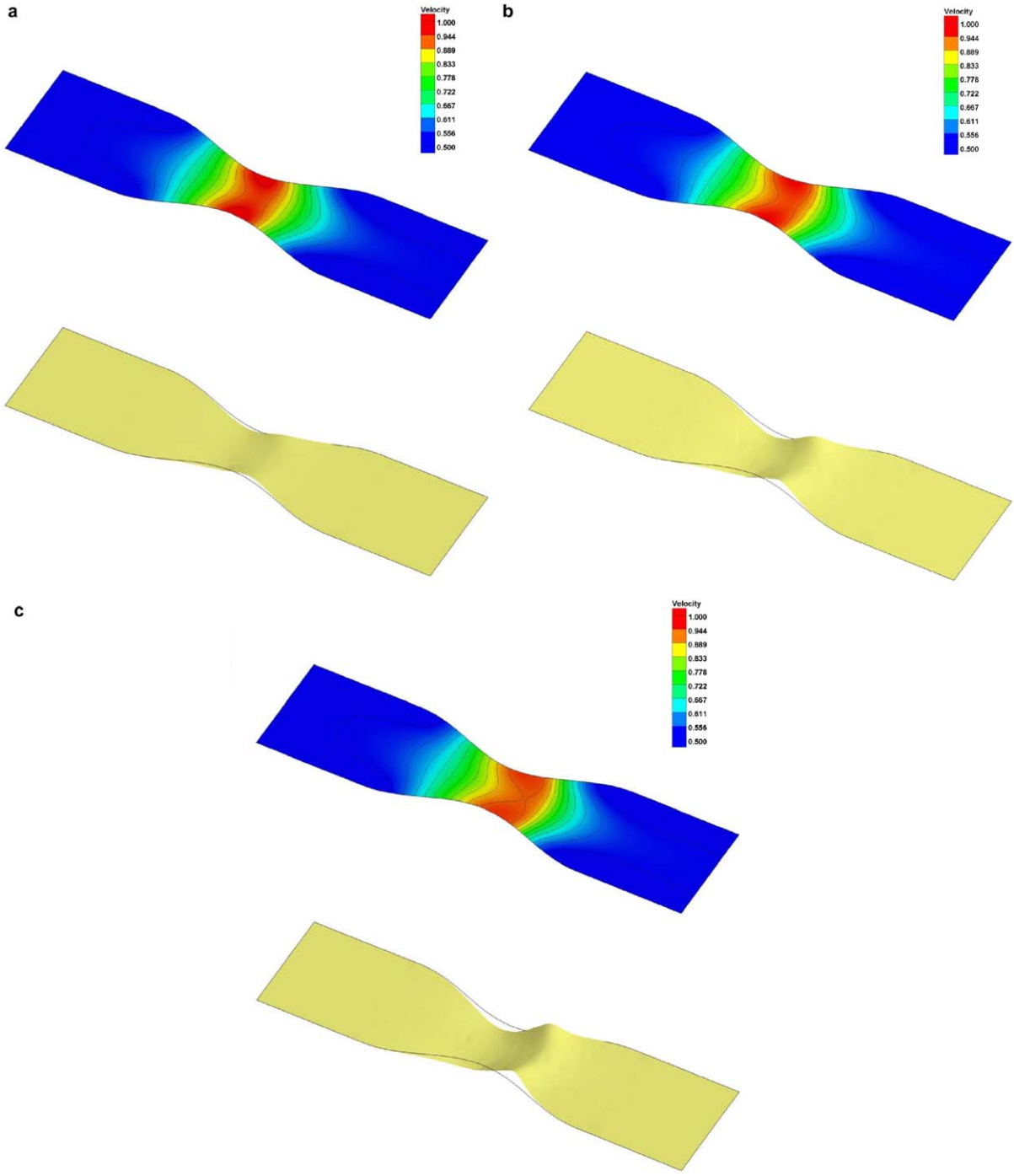

Fig. 9. Velocity contours and bed surface for test case 2—(a) Day 30; (b) Day 60; (c) Day 90.

The velocity throughout the channel varies from approximately 0.50 m/s at the ends of the channel to approximately 1 m/s in the center of the channel. The bed experiences erosion in the converging part of the channel due to the increase in the flow velocity. Conversely, in the diverging part of the channel, as the flow velocity decreases, accretion of the sediment occurs and a mound or shoal develops in time. It can be noted the scour and accretion patterns occurring in the center of the channel are slightly larger than those occurring toward the sides of the channel across the width of a given cross section. This can be explained by the fact that the velocity field is not entirely uniform across the width of the channel with somewhat higher velocities occurring in the center. These small variations in the velocity field across the width of the channel produce variations in the morphology of the bed across the width of the channel given the fact that the sediment transport is a function of $\mathbf{U}^3$. We also note that the velocity field evolves along with the morphological changes.

Finally, we remark that the computed results of the evolution of the bed compare well qualitatively to an analytical solution given by Exner (1925) for a problem of the same geometry. Exner's results, as shown in Fig. 10, are the solution of a simplified model similar to that of Section 2 but modified accordingly to account for variations in the width of the channel (see Graf, 1971 for details). Specifically, it can be seen that the numerical and analytical solutions show the same general evolution of the bed, i.e. scour in the converging section of the channel and accretion in the diverging section.

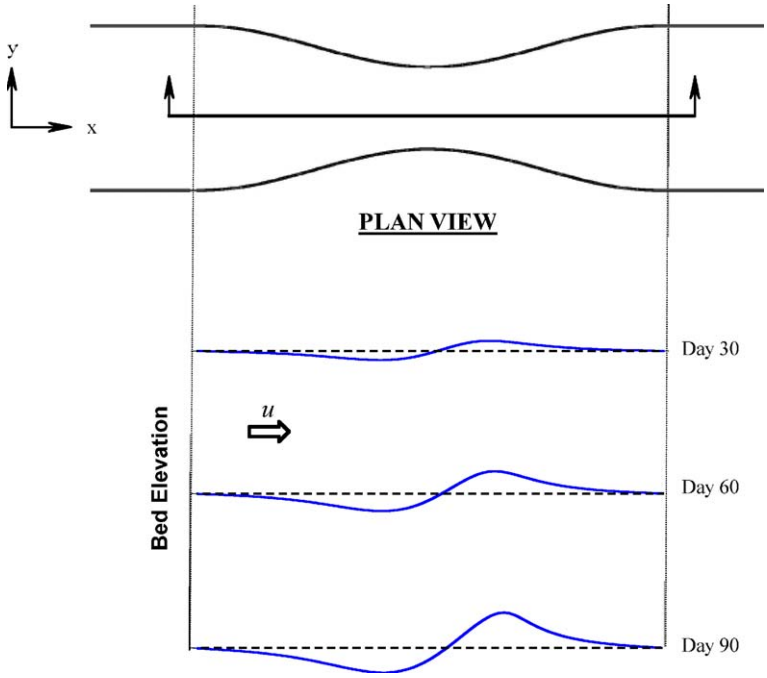

Fig. 10. Exner's analytical solution for the converging channel.

4.3. Test Case 3: Idealized inlet

In this problem, we apply the model to the case of an idealized inlet as shown in Fig. 11. The domain consists of a 10 km by 20 km sound connected to the open ocean through an inlet which is 1 km wide and 0.5 km long. The open ocean boundary is 20 km from the entrance of the inlet and is 50 km wide. The initial bathymetry in the sound and through the inlet is constant at a depth of 5 m. South of the inlet the bathymetry varies linearly from 5 m at the entrance to 14 m at the open ocean boundary. The sediment density and median grain size are the same as those specified in the previous problem. The grid for the problem is also shown in Fig. 11 with the inset showing the details in the vicinity of the inlet. The nodal spacing ranges from 100 m near the inlet to 1 km at the open ocean boundary. The problem is forced with an M_2 tide with a 15 cm amplitude which produces a maximum current of approximately 1 m/s through the inlet. The time step used for the hydrodynamics is 5 s, and the bed is updated every 50 hydrodynamic time steps. A 28-day simulation was run with magnified sediment transport rates in order to enhance the advective processes and accelerate the morphological evolution of the dominant features. Runs with no magnification of the sediment transport rates produced qualitatively similar results with smaller changes in the bed.

Figs. 12a–d show the time evolution of the bed every 7 days over the 28-day simulation. Note that larger values in the bed elevation indicate erosion and lower values indicate accretion due to the fact that the bed is measured as positive downward from the geoid. On day 7, there is noticeable erosion beginning at the southern end of the inlet. Accumulation of the sediment can be seen along the sides of the inlet and to the south of the inlet indicating the initial formation of an ebb shoal. During flood tide on day 14, it can be seen that there has been significant erosion through the throat of the inlet resulting in the initial formation of a flood shoal. It can also be seen that the ebb shoal has become more pronounced. By day 21, there are distinct flood and ebb shoals to the north and south of the inlet, respectively. There is also additional erosion through the inlet following the same pattern as the initial scour. At the end of day 28, there has been significant scour through the entire length of the inlet and the flood and ebb shoals have become even more pronounced. It should be noted that even at this level of coarse grid resolution the model captures the main morphological changes one expects to observe in tidally dominated coastal inlets (see for example Hayes, 1980).

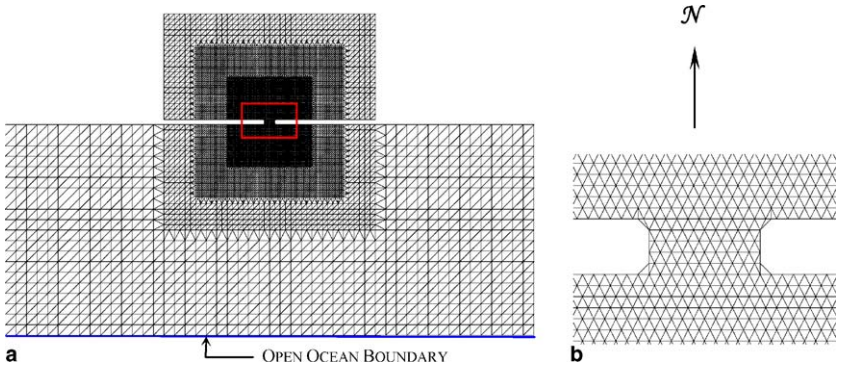

Fig. 11. (a) Computational grid for the idealized inlet of test case 3 and (b) details of the grid in the vicinity of the inlet.

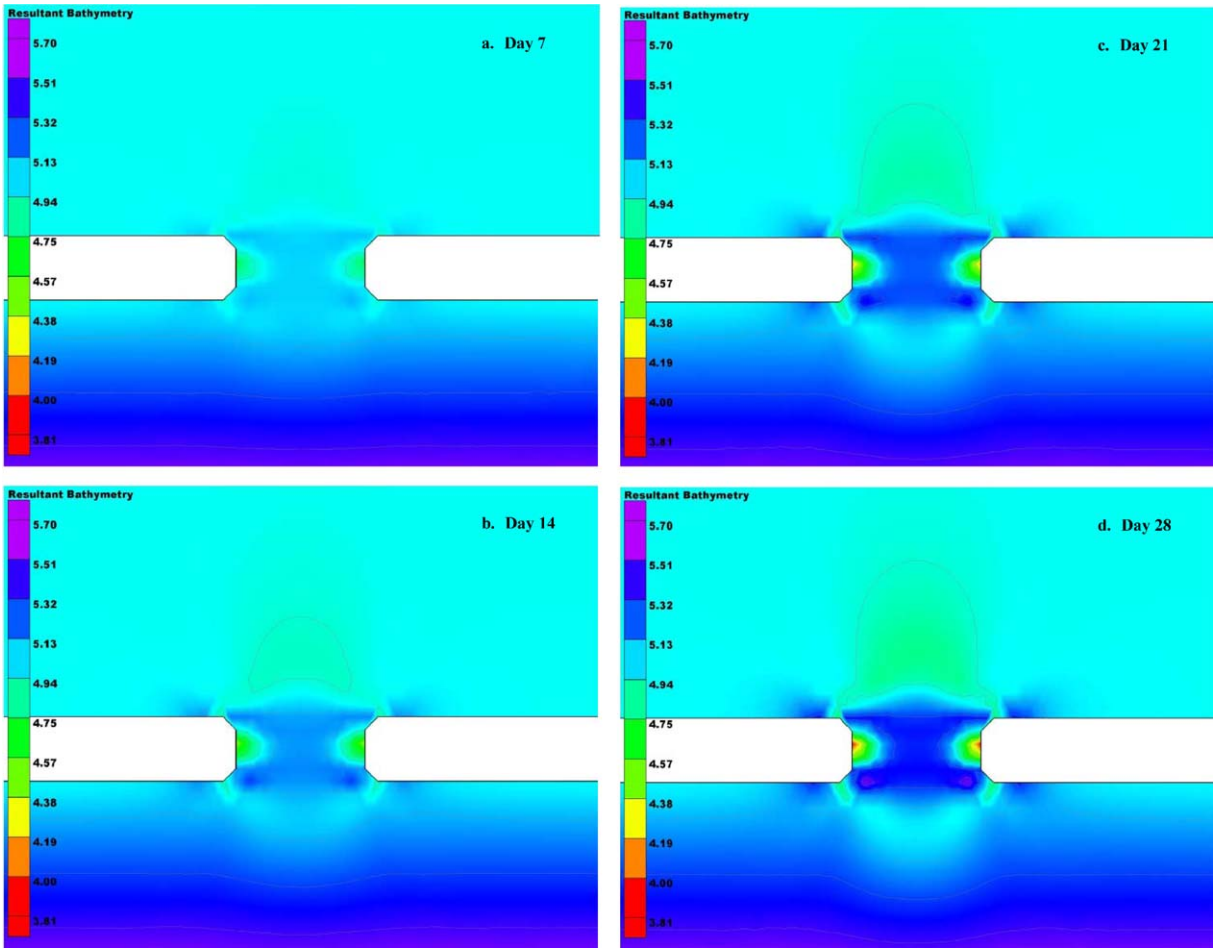

Fig. 12. Evolution of the bed in the vicinity of the inlet over the 28-day simulation—(a) Day 7, (b) Day 14, (c) Day 21, and (d) Day 28.

5. Summary and future work

In this paper, we have presented a new unstructured grid morphodynamic model which makes use of the existing ADCIRC finite element hydrodynamic model and a new DG finite element sediment transport/morphological model. Specific details were given on the implementation of the DG method, and the model was shown to produce good results in three idealized test cases. In the first test case it was verified, through the use of the Exner model, that the method achieves second-order convergence in space. Additionally, it was demonstrated how the DG method can accurately capture steep gradients in the bathymetry without the introduction of spurious spatial oscillations. The second and third test cases demonstrated how the full morphodynamic modelling system can be used to predict medium-term morphological changes of the bed in channels and tidally dominated coastal inlets.

We conclude with some comments on the current development of this morphodynamic modelling system, in terms of both physical and numerical features that will be implemented. In this paper, we have only considered sediment transport due to currents. However, in many coastal scenarios short waves, which interact with the current through the introduction of radiation stress terms in the momentum equations, can be the dominant force in the sediment transport process. Therefore, future work will involve coupling a wave model component into the modelling system to include the effects of waves in both the hydrodynamics and sediment transport processes. Numerically, as was previously indicated, the present model is only one component of a suite of DG models that are currently being developed. Other DG model components will include a 2DDI DG hydrodynamic model (see Kubatko et al., in preparation) and 2DDI DG transport models for salinity and temperature. In many applications, these models will be used in advection dominated flow scenarios such as coastal inlets. The DG method is particularly advantageous for these types of situations.

Acknowledgment

This work was supported by the US Army Engineer Research and Development Center under contracts DACW 42-00-C-0006 and W912HZ-05-0022 under the Coastal Inlets Research Program with Dr. Nicholas Kraus as technical leader and Ms. Mary Cialone as principal investigator.

References

Blain, C.A., Westerink, J.J., Luettich, R.A., 1994. The influence of domain size on the response characteristics of a hurricane storm surge model. Journal of Geophysical Research 99 (C9), 18467–18479.

Camenen, B., Larson, M., 2005. A general formula for non-cohesive bed load sediment transport. Estuarine, Coastal, and Shelf Science 63 (1–2), 249–260.

Cockburn, B., Shu, C.-W., 1998. The Runge–Kutta discontinuous Galerkin finite element method for conservation laws V: multidimensional systems. Journal of Computational Physics 141 (2), 199–224.

Cockburn, B., Shu, C.-W., 2001. Review article: Runge–Kutta discontinuous Galerkin methods for convection-dominated problems. Journal of Scientific Computing 16 (3), 173–261.

Crouzeix, M., Raviart, P.-A., 1973. Conforming and nonconforming finite element methods for solving the stationary Stokes equations I. RFAIRO: Analyse numerique 7 (R-3), 33–76.

Dawson, C., Sun, S., Wheeler, M.F., 2004. Compatible algorithms for coupled flow and transport. Computer Methods in Applied Mechanics and Engineering 193 (23–26), 2565–2580.

De Vriend, H.J., Zyserman, J., Nicholson, J., Roelvink, J.A., Pechon, P., Southgate, H.N., 1993. Medium-term 2DH coastal area modeling. Coastal Engineering 21 (1–3), 193–224.

Dubiner, M., 1991. Spectral methods on triangles and other domains. Journal of Scientific Computing 6 (4), 345–390.

Exner, F.M., 1925. Uber die wechselwirkung zwischen wasser und geschiebe in flussen. Sitzungsberichte der Akademie der Wissenschaften Wien. 165 (3–4), 165–203.

Graf, W.H., 1971. Hydraulics of Sediment Transport. McGraw-Hill Book Company, New York.

Hayes, M.O., 1980. General morphology and sediment patterns in tidal inlets. Sedimentary Geology 26 (1–3), 139–156.

Henderson, F.M., 1966. Open Channel Flow. MacMillan Publishing Company, New York.

Iskandarani, M., Levin, J.C., Choi, B.-J., Haidvogel, D.B., 2005. Comparision of advection schemes for high-order h–p finite element and finite volume methods. Ocean Modelling 10 (1–2), 233–252.

Johnson, Hakeem K., Zyserman, Julio A., 2002. Controlling spatial oscillations in bed level update schemes. Coastal Engineering 46 (2), 109–126.

Kinnmark, I., 1986. The Shallow Water Wave Equations: Formulation, Analysis, and Application. Lecture Notes in Engineering. Springer-Verlag, New York.

Kubatko, E.J., Westerink, J.J., Dawson, C., in preparation. *hp* discontinuous Galerkin methods for advection dominated problems in shallow water flow.

Luettich, R.A., Westerink, J.J, 2004. Formulation and Numerical Implementation of the 2D/3D ADCIRC finite element model version 44.XX. Available from: <http://www.marine.unc.edu/C_CATS/adcirc/adcirc_theory_2004_05_14.pdf>.

Lynch, D.R., Gray, W.G., 1979. A wave equation model for finite element tidal computations. Computers and Fluids 7 (3), 207–228.

Mukai, A., Westerink, J.J., Luettich, R.A., Mark, D.J. 2002. A tidal constituent database for the western north Atlantic Ocean, Gulf of Mexico and Caribbean Sea. Technical Report, US Army Engineer Research and Development Center, Vicksburg MS, Report ERDC/CHL TR-02-24.

Nicholson, J., Broker, I., Roelvink, J.A., Price, D., Tanguy, J.M., Moreno, L., 1997. Intercomparision of coastal area morphodynamic models. Coastal Engineering 31 (1–4), 97–123.

Reed, W.H., Hill, T.R., 1973. Triangular mesh methods for the neutron transport equation. Technical Report LA-UR-73-479, Los Alamos Scientific Laboratory.

Sleath, J.F.A., 1984. Sea Bed Mechanics. John Wiley & Sons, New York.

Soulsby, R., Whitehouse, R., 1997. Threshold of sediment motion in coastal environment. Proceedings Pacific Coasts and Ports 1997 Conference. University of Canterbury, Christchurch, New Zealand, pp. 149–154.

Westerink, J.J., Feyen, J.C. , Atkinson, J.H., Luettich, R.A., Dawson, C.N., Powell, M.D., Dunion, J.P., Roberts, H.J., Kubatko, E.J., Pourtaheri, H., in review. A new generation hurricane storm surge model for southern Louisiana. Bulletin of the American Meteorological Society.

Westerink, J.J., Luettich, R.A., Muccino, J.C, 1994. Modeling tides in the western north Atlantic using unstructured graded grids. Tellus 46A, 178–199.